

# Unusual Magnetic, Thermal, and Transport Behaviors of Single Crystal $\text{EuRh}_2\text{As}_2$

Yogesh Singh, Y. Lee, B. N. Harmon, and D. C. Johnston

Ames Laboratory and Department of Physics and Astronomy, Iowa State University, Ames, Iowa 50011

(Dated: November 5, 2018)

An *antiferromagnetic* transition is observed in single crystal  $\text{EuRh}_2\text{As}_2$  at a high temperature  $T_N = 47$  K compared to the *ferromagnetic* Weiss temperature  $\theta = 12$  K. We show that this is, surprisingly, consistent with mean field theory. A first-order field-induced magnetic transition is observed at  $T < T_N$  with an unusual temperature dependence of the transition field. A dramatic magnetic field-induced reduction of the electronic specific heat coefficient at 1.8–5.0 K by 38% at 9 T is observed. In addition, a strong positive magnetoresistance and a large change in the Hall coefficient occur below 25 K. Band structure calculations indicate that the Fermi energy lies on a steep edge of a narrow peak in the density of states.

The recent discovery of superconductivity with transition temperatures up to  $T_c = 38$  K in the layered iron arsenides  $A\text{Fe}_2\text{As}_2$  ( $A = \text{Ba}, \text{Sr}, \text{Ca}, \text{and Eu}$ ) when the  $A$  atoms are partially replaced by K (Ref. 1) has led to a renewed interest in  $\text{ThCr}_2\text{Si}_2$ -structure materials. We have been carrying out a search of similar isostructural compounds such as  $\text{Ba}(\text{Rh}, \text{Mn})_2\text{As}_2$  (Ref. 2) in an attempt to significantly increase the maximum  $T_c$  for this class of compounds. Nature provided a gift of a different sort when we studied the physical properties of another member<sup>3</sup> of this structure class,  $\text{EuRh}_2\text{As}_2$ , and found a variety of novel behaviors as reported here.

Our primary results are as follows. First, from our anisotropic magnetic susceptibility  $\chi$  versus temperature  $T$  data on  $\text{EuRh}_2\text{As}_2$  single crystals, the Eu ions are found to have an intermediate valence 2.13(2) unusually close<sup>4</sup> to  $\text{Eu}^{+2}$ , which has a spin-only magnetic moment with  $J = S = 7/2$ . Second, an unusually large *antiferromagnetic* ordering temperature  $T_N = 47$  K compared to the *ferromagnetic* (positive) Weiss temperature  $\theta \approx 12$  K is found. It is widely assumed that the magnitude of  $\theta$  in the Curie-Weiss law  $\chi = C/(T - \theta)$  is the mean-field transition temperature for either ferromagnetic FM or antiferromagnetic AF ordering of a local moment system, which is the maximum transition temperature that the system can have. Magnetic fluctuations and frustration effects reduce the magnetic ordering temperature below the mean-field value, so our observation that  $T_N/|\theta| \approx 4 \gg 1$  is surprising. The resolution of this conundrum is simple: mean-field theory for a local moment antiferromagnet in fact *allows arbitrarily large values* of the ratio  $T_N/|\theta|$ .<sup>5</sup> This can happen in an antiferromagnet when FM exchange interactions between spins within the same sublattice exist, in addition to the usual AF interactions between spins on opposite sublattices.

Third, a very unusual and dramatic monotonic magnetic field-induced reduction of the electronic specific heat coefficient  $\gamma$  is observed at 1.8–5.0 K by 38% at a relatively low field of 9 T. We suggest that field-induced stabilization<sup>4</sup> of the +2 valence of Eu is centrally involved. Finally, a strong positive magnetoresistance develops below 25 K that violates Kohler's rule, where  $\rho(T)$  shows a “nonmetallic” increase with decreasing  $T$  at fixed  $H$ , together with a large change in the Hall coefficient be-

low 25 K. These apparently coupled electronic behaviors have no obvious origin. Our band structure calculations indicate that the Fermi energy lies on a steep edge of a sharp peak in the density of states.

Single crystals of  $\text{EuRh}_2\text{As}_2$  were grown out of Pb flux.<sup>3</sup> Single crystal x-ray diffraction measurements confirmed that  $\text{EuRh}_2\text{As}_2$  crystallizes in the tetragonal  $\text{ThCr}_2\text{Si}_2$  structure with lattice parameters  $a = 4.075(4)$  Å and  $c = 11.295(2)$  Å at 298 K. The compositions of two crystals were determined using energy dispersive x-ray analysis, yielding the average atomic ratios  $\text{Eu}:\text{Rh}:\text{As} = 20.8 : 37.9 : 41.3$ . The  $\chi(T)$  and magnetization  $M$  versus applied magnetic field  $H$  isotherms were measured with a Quantum Design MPMS SQUID magnetometer. The  $\rho(T)$ ,  $C(T)$  and Hall effect were measured using a Quantum Design PPMS instrument.

For the electronic density of states (DOS) calculations, we used the full potential linearized augmented plane wave method with a local density approximation functional.<sup>6</sup> The difference in energy of 0.01 mRy/cell between successive iterations was used as a convergence criterion. The employed muffin tin radii are 2.5, 2.2 and 2.2 atomic units for Eu, Rh, and As, respectively.  $4f$  electrons of Eu were treated as core electrons. The structural data were taken from Ref. 3. The total DOS for both spin directions for  $\text{EuRh}_2\text{As}_2$  and the partial DOS for Eu  $5d$ , Rh  $4d$  and As  $4p$  electrons versus the energy  $E$  relative to the Fermi energy  $E_F$  are shown in Fig. 1.  $E_F$  is located just below an extremely sharp peak in the DOS. The total DOS at  $E_F$  is  $N(E_F) = 3.38$  states/eV f.u. (f.u. means formula unit) for both spin directions with maximum contribution from the Rh  $4d$  orbitals.

The  $\chi(T)$  data for a crystal of  $\text{EuRh}_2\text{As}_2$  measured with  $H$  parallel ( $\chi_c$ ) and perpendicular ( $\chi_{ab}$ ) to the  $c$  axis are shown in Fig. 2. The powder-averaged susceptibility  $\chi_{\text{powder}} = (2\chi_{ab} + \chi_c)/3$  is also shown in Fig. 2. The  $\chi_{\text{powder}}(T)$  data above 60 K were fitted by the expression  $\chi(T) = f\chi_{\text{Eu}^{+3}}(T) + (1 - f)C/(T - \theta)$ , where the Van Vleck susceptibility  $\chi_{\text{Eu}^{+3}}(T)$  of  $\text{Eu}^{+3}$  is given in Ref. 7,  $C$  is the Curie constant for  $\text{Eu}^{+2}$  with  $g$ -factor  $g = 2$ ,<sup>8</sup> and  $\theta$  is the Weiss temperature for interactions between  $\text{Eu}^{+2}$  moments. An excellent fit was obtained with  $f = 0.13(2)$  and  $\theta = 12(2)$  K (inset). An average valence of 2.13(2) is therefore obtained for Eu. This is different

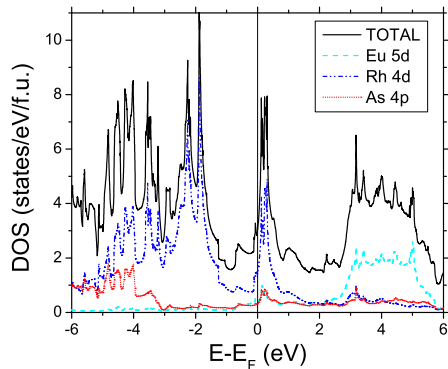


FIG. 1: The total density of states DOS for  $\text{EuRh}_2\text{As}_2$  versus energy  $E$  relative to the Fermi energy  $E_F$  and the partial DOS versus  $E$  from the Eu, Rh, and As atoms.

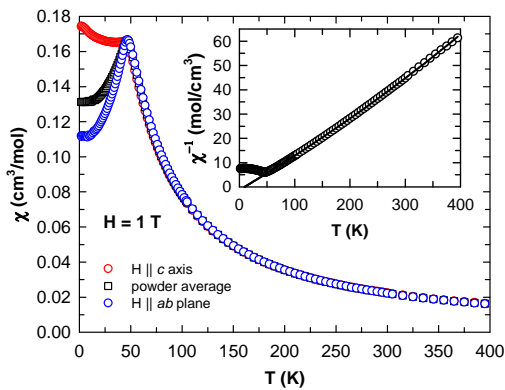


FIG. 2:  $\chi_{ab}$  and  $\chi_c$  versus temperature  $T$  for  $\text{EuRh}_2\text{As}_2$ . The powder-averaged  $\chi_{\text{powder}}$  is also shown. Inset: fit (solid curve) of the  $\chi^{-1}(T)$  data (open circles), see text.

from the value  $\approx 2.00$  obtained for  $\text{EuRh}_2\text{As}_2$  in Ref. 9, possibly due to composition differences of the samples.

The positive value  $\theta = 12$  K indicates predominantly *ferromagnetic* exchange interactions between the magnetic  $\text{Eu}^{2+}$  moments. Surprisingly, however, in Fig. 2 we observe a sharp decrease in  $\chi_{ab}$  indicating a transition into an *antiferromagnetic* state at a much *higher* Néel temperature  $T_N = 47$  K. The  $\chi_c$  also shows an abrupt change in slope at  $T_N$  and becomes weakly temperature dependent at lower  $T$ . The large value of  $\chi_{ab}(T \rightarrow 0)$  indicates that  $\text{EuRh}_2\text{As}_2$  is a noncollinear easy plane antiferromagnet with the easy plane being the *ab* plane. Magnetic x-ray scattering measurements on our crystals at  $H = 0$  revealed both commensurate and incommensurate magnetic structures in which the Eu spins are ferromagnetically aligned within the *ab* plane and where the spins in adjacent planes are, or are nearly, antiparallel.<sup>10</sup>

A large ratio of  $T_N/|\theta|$  can occur within mean-field theory for a two-sublattice collinear antiferromagnet with equal numbers of spins on the two sublattices, each with Curie constant  $C/2$ , as follows. A spin in each sublattice

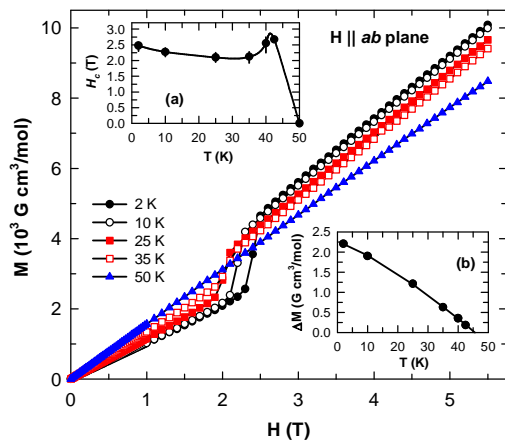


FIG. 3:  $M(H)$  at various  $T$  with  $H$  applied parallel to the *ab* plane. Inset(a): metamagnetic field  $H_c$  versus  $T$ . The vertical bars on the data points are the widths of the metamagnetic transition. The solid curve is a guide to the eye. Inset(b): change in magnetization  $\Delta M$  at the transition versus  $T$ .

is assumed to interact with the same number of spins both within its own sublattice and with the other sublattice with mean-field coupling constants  $\lambda_1$  and  $\lambda_2$ , respectively. Applying the usual mean-field treatment one obtains the Weiss temperature  $\theta = C(\lambda_1 + \lambda_2)/2$  and magnetic ordering temperature  $T_N = C(\lambda_1 - \lambda_2)/2$ . Thus

$$\frac{T_N}{\theta} = \frac{\lambda_1 - \lambda_2}{\lambda_1 + \lambda_2} = \frac{\mathcal{J}_1 - \mathcal{J}_2}{\mathcal{J}_1 + \mathcal{J}_2}, \quad (1)$$

where  $\mathcal{J}_1$  and  $\mathcal{J}_2$  are the nearest-neighbor exchange coupling constants for two spins in the same and different sublattices, respectively. If  $\lambda_1, \mathcal{J}_1 > 0$  (FM) and  $\lambda_2, \mathcal{J}_2 < 0$  (AF), one can obtain arbitrarily large values of the ratio  $T_N/|\theta|$ . For our case with  $T_N/\theta \approx 4$ , Eq. (1) yields  $\lambda_1/\lambda_2 = \mathcal{J}_1/\mathcal{J}_2 \approx -5/3$ .

$M(H)$  isotherms at various  $T$  with  $H$  applied along the *ab* plane are shown in Fig. 3. The  $M(H)$  data for  $H \parallel c$  (not shown) are proportional at all temperatures from 2 to 300 K. The  $M(H)$  data for  $H$  applied along the *ab* plane are also proportional for temperatures  $T > T_N = 47$  K as seen in Fig. 3. However, for  $T < T_N$  the  $M(H)$  is initially proportional but then shows a first-order step-like increase in  $M$  at a metamagnetic critical field  $H_c$  which exhibits hysteresis (not shown) upon increasing and decreasing  $H$ . Above  $H_c$ ,  $M$  again is proportional to  $H$  but with a larger slope. The value of  $M$  at  $T = 2$  K and  $H = 5.5$  T is only  $1.81 \mu_B/\text{f.u.}$ , which is much smaller than the expected  $\text{Eu}^{2+}$  saturation moment  $7.0 \mu_B/\text{Eu}$ . Our data thus indicate that a first-order transition between two antiferromagnetically ordered states occurs at  $H_c$ . Figure 3 inset(a) shows that  $H_c$  decreases initially with increasing  $T$  between 2 K and 25 K, as expected, but then increases strongly on further approaching  $T_N$ . At  $T = 50$  K  $> T_N$  we did not observe any metamagnetic transition. The increase in magnetization  $\Delta M$  across the metamagnetic transition versus  $T$  is

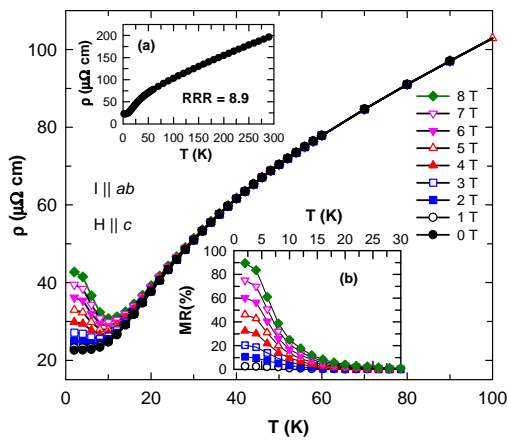


FIG. 4: Resistivity  $\rho$  in the  $ab$  plane versus temperature  $T$  measured in various  $H \parallel c$ . Inset (a):  $\rho(T)$  for  $H = 0$ . Inset (b): Magnetoresistance MR below  $T = 30$  K.

shown in Fig. 3 inset(b). In contrast to  $H_c$ ,  $\Delta M$  shows a monotonic decrease with  $T$  and vanishes near  $T_N$  as expected.

The  $\rho(T)$  data for current in the  $ab$  plane for  $H = 0$  and for temperatures from 2 K to 300 K are shown in Fig. 4 inset(a). These data indicate metallic behavior with a residual resistivity ratio  $RRR = \rho(300 \text{ K})/\rho(2 \text{ K}) = 8.9$ . There is no sudden reduction in  $\rho(T)$  below  $T_N = 47$  K as might be expected below a magnetic ordering transition due to a reduction of spin-disorder scattering. This is particularly surprising in view of the sharp transitions at  $T_N$  seen in  $\chi(T)$  and  $C(T)$  in Fig. 2 and in Fig. 6 below, respectively.

The field-dependent  $\rho(T, H)$  data are shown in Fig. 4 between 2 K and 100 K. A strong increase in  $\rho$  occurs with increasing  $H$  beginning below 25 K. The magnetoresistance percentage values  $MR(H, T) \equiv 100[\rho(H, T) - \rho(0, T)]/\rho(0, T)$  versus  $T$  at various  $H$  are shown in Fig. 4 inset(b). A large MR is seen at low  $T$  with increasing  $H$ : the MR reaches 90% at  $T = 2$  K and  $H = 8$  T. From the single-band relation  $\omega_c \tau = |R_H|H/\rho$ , where  $\omega_c$  is the cyclotron frequency,  $\tau$  is the mean-free scattering time of the current carriers and  $R_H$  is the Hall coefficient, and using our experimental  $R_H$  (below) and  $\rho$  data at 2 K, one finds that our MR data are in the low-field regime  $\omega_c \tau \sim 0.003 \ll 1$  at 8 T. In this regime one normally expects<sup>11</sup>  $MR \sim H^2$  instead of the different behavior we observe in Fig. 5 inset. A positive MR can occur due to increased spin-disorder scattering upon suppression of an antiferromagnetic ordering by a magnetic field.<sup>12</sup> However, this explanation is untenable here because as shown in Fig. 6 below, the  $T_N$  of  $\text{EuRh}_2\text{As}_2$  is suppressed to only  $\sim 40$  K in  $H = 8$  T. Furthermore, one expects a zero MR with  $H \parallel c$  ( $H \perp$  ordered moment direction) due to AF fluctuations at  $T \ll T_N$ .<sup>13</sup> According to semiclassical transport theory, the MR follows Kohler's rule  $MR = F[H/\rho(0)]$ , where  $F(x)$  is a universal function for a given material, if there is a single species of charge car-

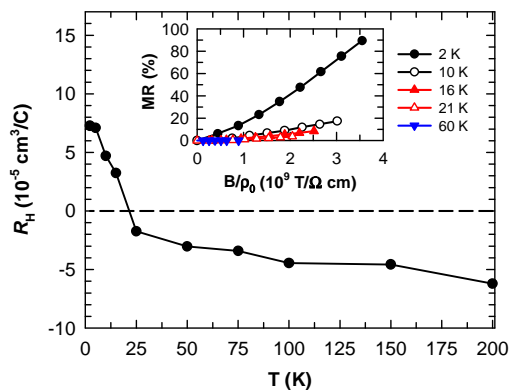


FIG. 5: Hall coefficient  $R_H$  vs.  $T$  for  $\text{EuRh}_2\text{As}_2$ . Inset: Magnetoresistance MR versus  $H/\rho(H = 0)$  at various  $T$ .

rier and the scattering time is the same at all points on the Fermi surface.<sup>11</sup> As shown in Fig. 5 inset, the MR in  $\text{EuRh}_2\text{As}_2$  severely violates Kohler's rule.

The Hall coefficient  $R_H$  was found to be independent of  $H$  up to 8 T and is plotted versus  $T$  at  $H = 8$  T in Fig. 5.  $R_H$  is negative and increases slowly with decreasing  $T$  from 200 K to 25 K, but then increases rapidly below 25 K, the temperature below which the MR also begins to strongly increase. An unusual  $T$  dependence of  $R_H$  is sometimes seen across a magnetic transition.<sup>14</sup> However, the strong increase in  $R_H$  for  $\text{EuRh}_2\text{As}_2$  occurs below 25 K which is well below  $T_N(H)$  as shown next.

The  $C(T)$  of a single crystal of  $\text{EuRh}_2\text{As}_2$  measured between 1.8 K and 70 K in various  $H \parallel c$  is shown in Fig. 6. For  $H = 0$ , a second-order anomaly with an onset at 48.3 K and a peak at 44.3 K is observed, from which we estimate  $T_N \approx 46$  K in agreement with the  $T_N$  found from our  $\chi(T)$  data above. The  $C(T)$  data for a single crystal of  $\text{BaRh}_2\text{As}_2$ ,<sup>2</sup> also shown in Fig. 6, were used to estimate the lattice heat capacity of  $\text{EuRh}_2\text{As}_2$ . Figure 6 inset(a) shows  $\Delta C(T)$  versus  $T$  between 2 K and 100 K, obtained by subtracting the heat capacity of  $\text{BaRh}_2\text{As}_2$ , adjusted for the molar mass difference with  $\text{EuRh}_2\text{As}_2$ , from that of  $\text{EuRh}_2\text{As}_2$ .  $\Delta C(T)$  is consistent with a mean-field transition at  $T_N$  as follows. In mean-field theory, the magnitude of the heat capacity jump at  $T_N$  is given by  $\Delta C(T_N) = \frac{5}{2}R \frac{(2S+1)^2 - 1}{(2S+1)^2 + 1} = 16.2 \text{ J/mol K}^2$  for  $S = 7/2$ ,<sup>15</sup> where  $R$  is the gas constant. This value is close to that observed in Fig. 6 inset(a). Furthermore, the entropy difference  $\Delta S(T)$  versus  $T$  obtained by integrating the  $\Delta C(H = 0, T)/T$  versus  $T$ , as shown in Fig. 6 inset(a), reaches the value  $R \ln 8$  expected for  $\text{Eu}^{2+}$  moments ( $J = S = 7/2$ ) just above  $T_N$  after which it becomes nearly  $T$  independent. From the  $C(T, H)$  data, one sees that  $T_N$  decreases by only  $\sim 5$  K at 8 T. Thus we infer that the strong positive MR below  $\sim 25$  K in Fig. 4 does not result from suppression of  $T_N$  to these low temperatures.

At 1.8–5.0 K, the heat capacity of  $\text{EuRh}_2\text{As}_2$  obeys  $C(T, H) = \gamma(H)T + \beta T^3$ , where  $\beta \approx 7.1(1) \text{ mJ/mol K}^4$  is independent of  $H$  and the electronic specific heat co-

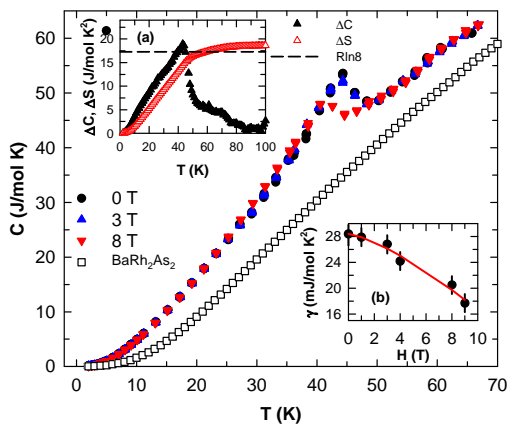


FIG. 6: Heat capacity  $C$  vs.  $T$  of single crystal  $\text{EuRh}_2\text{As}_2$  at various  $H \parallel c$ , and for single crystal  $\text{BaRh}_2\text{As}_2$  in  $H = 0$ . Inset (a):  $\Delta C(T)$  and  $\Delta S(T)$  vs.  $T$ . The dashed horizontal line is the value  $\Delta S = R \ln 8$  expected for disordered  $\text{Eu}^{2+}$  ( $J = S = 7/2$ ) spins. Inset (b):  $\gamma$  versus  $H$ .

efficient  $\gamma(H)$  is plotted in Fig. 6 inset(b). Between  $H = 0$  T and 9 T,  $\gamma$  decreases monotonically from 28.4(9) mJ/mol K<sup>2</sup> to 17.7(7) mJ/mol K<sup>2</sup>, a remarkable reduction of 38%. This reduction in  $\gamma$  might be explained by a field-induced carrier localization; however, the field-independence of  $R_H$  (above) argues against such an interpretation. From  $N(E_F) = 3.38$  states/eV f.u. obtained above from our band structure calculations for a valence  $\text{Eu}^{+2}$ , we obtain  $\gamma = 7.96$  mJ/mol K<sup>2</sup> assuming zero electron-phonon coupling. This value is about 3.5 times smaller than the observed zero-field value. This discrepancy suggests that the high observed  $\gamma(H = 0)$  is due to the intermediate valence 2.13(2) of Eu inferred from  $\chi(T)$  above  $T_N$ ,<sup>16</sup> and that the field-induced reduction in  $\gamma$  towards the band structure value arises from field-induced stabilization<sup>4</sup> of the Eu valence towards  $\text{Eu}^{+2}$  and concomitant reduction in the spin fluctuation<sup>16</sup> contribution.

In summary, our magnetic, transport, and thermal

measurements on single crystals of  $\text{EuRh}_2\text{As}_2$  revealed an array of interesting and unusual behaviors. From  $\chi(T)$  measurements at temperatures  $T > T_N$ , the Eu ions are found to have an intermediate valence 2.13(2) unusually close<sup>4</sup> to  $\text{Eu}^{+2}$ . The large ratio  $T_N/\theta \approx 4$  is very unusual. A simple two-sublattice mean-field model where each sublattice interacts with itself in addition to the other explains how  $T_N/|\theta| > 1$  can come about. Other relevant examples of antiferromagnets where  $T_N/|\theta| > 1$  have been reported,<sup>5,17,18,19</sup> although the authors did not take specific note of this ratio. For  $\text{LaMnO}_3$ , using Eq. (1) and the  $\mathcal{J}_{1,2}$  values in Ref. 20, one obtains the mean-field ratio  $T_N/\theta = 3.8$ , slightly larger (as expected) than the observed value of 3.0 obtained from  $\theta = 46$  K and  $T_N = 140$  K.<sup>19</sup> In retrospect, it is surprising that antiferromagnets with  $T_N/|\theta| > 1$  are not more commonly observed. The temperature variation of the metamagnetic field  $H_c$  as  $T_N$  is approached is anomalous. The strong decrease in the electronic heat capacity coefficient  $\gamma$  with  $H$  at relatively low fields up to 9 T is very unusual.<sup>21</sup> In most metals,  $\gamma$  is independent of  $H$  in such fields because the magnetic field energy of a conduction carrier is far smaller than the Fermi energy. We suggest that the observed  $\gamma(H)$  results from a field-induced stabilization<sup>4</sup> of the Eu valence towards  $\text{Eu}^{+2}$  at low  $T$ . This hypothesis can be checked using, *e.g.*, x-ray absorption spectroscopy (XAS).<sup>4</sup> A strong positive magnetoresistance and a strong increase in  $R_H$  develop below 25 K suggesting a possible temperature-induced redistribution of carriers between electron- and hole-like Fermi surfaces, which can be tested using angular-resolved photoemission spectroscopy (ARPES).

### Acknowledgments

We thank S. Nandi, A. Kreyssig, A. I. Goldman and J. Schmalian for helpful discussions and A. Ellern for structure analysis. Work at Ames Laboratory was supported by the Department of Energy-Basic Energy Sciences under Contract No. DE-AC02-07CH11358.

<sup>1</sup> For a review, see M. V. Sadovskii, arXiv:0812.0302 (2008).  
<sup>2</sup> Y. Singh *et al.*, Phys. Rev. B **78**, 104512 (2008); arXiv:0901.3370 (2009).  
<sup>3</sup> A. Hellmann *et al.*, Z. Naturforsch. **62b**, 155 (2007).  
<sup>4</sup> Y. H. Matsuda *et al.*, J. Phys. Soc. Jpn. **77**, 054713 (2008).  
<sup>5</sup> We exclude cases where  $\theta$  arises from single-ion effects.  
<sup>6</sup> J. P. Perdew and Y. Wang, Phys. Rev B **45**, 13244 (1992).  
<sup>7</sup> J. H. Van Vleck, *The Theory of Electric and Magnetic Susceptibilities* (Clarendon, Oxford, 1932), p. 248.  
<sup>8</sup> R. H. Taylor and B. R. Coles, J. Phys. F **5**, 121 (1975).  
<sup>9</sup> G. Michels *et al.*, J. Phys.: Condens. Matter **8**, 4055 (1996).  
<sup>10</sup> S. Nandi *et al.*, unpublished.  
<sup>11</sup> A. B. Pippard, *Magnetoresistance in Metals*, 1st edition (Cambridge University Press, Cambridge, 1989).

<sup>12</sup> Z. Ren *et al.*, Phys. Rev. B, **78**, 052501 (2008).  
<sup>13</sup> H. Yamada and S. Takada, J. Phys. Soc. Jpn. **34**, 51 (1973).  
<sup>14</sup> C. M. Hurd, *The Hall Effect in Metals and Alloys* (Plenum Press, New York, 1972).  
<sup>15</sup> J. S. Smart, *Effective Field Theories of Magnetism* (W. B. Saunders Company, Philadelphia, 1966).  
<sup>16</sup> C. M. Varma, Rev. Mod. Phys. **48**, 219 (1976).  
<sup>17</sup> E. M. Levin *et al.*, Phys. Rev. B **69**, 144428 (2004).  
<sup>18</sup> S. L. Bud'ko *et al.*, J. Magn. Magn. Mater. **205**, 53 (1999).  
<sup>19</sup> M. R. Ibarra *et al.*, Phys. Rev. B **56**, 8902 (1997).  
<sup>20</sup> R. J. McQueeney *et al.*, Phys. Rev. B **78**, 184417 (2008).  
<sup>21</sup> See also Y. Aoki *et al.*, J. Phys. Soc. Jpn. **65**, 1005 (1996).